# Direct Numerical Simulation of Microbubble Dynamics in Turbulent Channel Flow

Jian Zhai, Michael Fairweather, Marco Colombo

School of Chemical and Process Engineering

University of Leeds, Leeds LS2 9JT, United Kingdom

pmjzhai@leeds.ac.uk; m.fairweather@leeds.ac.uk; m.colombo@leeds.ac.uk

**Keywords**: Direct numerical simulation, microbubbles, turbulence modulation, bubble coalescence

**Abstract**

This work investigates microbubble dynamics in four-way (with coalescence) coupled microbubble-laden turbulent channel flows. Both upflow and downflow of water at a shear Reynolds number $Re_\tau$ = 150 are considered, where microbubbles, assumed to be non-deformable and spherical, are injected and tracked using a Lagrangian approach. One-way and two-way coupled predictions, used to successfully validate the model, demonstrate different trends in bubble preferential motion. Four-way coupled simulations with coalescence clearly demonstrate that the presence of the bubbles, and collisions between them, have a non-negligible effect on the fluid phase. Simulation results indicate that binary bubble collisions occur at very small angles between the two velocity vectors, and with low relative approaching velocities generally favoured. Special attention is paid to the performance of different bubble coalescence closures, with the film drainage model returning a 100% coalescence efficiency. In contrast, the energy model returns a 0% coalescence efficiency, and this large discrepancy between available coalescence models requires further investigation. The knowledge gained on the mechanisms that underpin bubble collisions is of value for the further development of coalescence closure models.

## Introduction

Dispersed bubbly flows consist of a population of gas bubbles dispersed in a liquid continuum. Bubbly flows of different kinds are found in a number of natural phenomena and are also widely used in engineering applications (Balachandar & Eaton 2010). In nuclear power plants cooled by water, bubbly flows are commonly encountered when boiling occurs, generating a large number of bubbles on the heated walls (Todreas & Kazimi, 2011). Also, bubble columns are widely used in chemical and petrochemical reaction units since they remove the need for moving parts and have good hydrodynamic and mass/heat transfer characteristics, even with large liquid holdup (Shah et al. 1982; Lau et al. 2013). The complexity of bubbly flows derives from bubble interactions with the turbulent fluid flow. When the gas void fraction increases above 3%, bubble-bubble interactions are no longer negligible (Elghobashi 1994). These interactions promote bubble coalescence, with turbulence leading to bubble break-up, and these phenomena determine the bubble size distribution within the flow and make the accurate prediction of bubbly flows in practical applications particularly challenging.

With the development of high performance computing (HPC) platforms in recent years, numerical simulations are now capable of resolving details of complex fluid mechanic processes that are difficult to capture even with the most advanced experimental techniques. Over the years, various advanced computational fluid dynamics methods have been developed to simulate and better understand the dynamics of turbulent bubbly flows.

Of the methodologies available, Eulerian-Lagrangian approaches treat the continuous phase in an Eulerian framework and the motion of individual or groups of bubbles is simulated by solving Newton's second law of motion by accounting for the forces acting on each bubble. By incorporating bubble-fluid and bubble-bubble interactions (e.g. bubble coalescence and break-up), the method provides a way to simulate phase interaction with a much higher spatial resolution than other methods such as Eulerian-Eulerian approaches. On the other hand, the bubbles are considered as points, which means that they should be smaller than the smallest resolved turbulence scale. In addition, closure relations for the interphase forces are required, and these are still mainly based on empirical relations from experiments. However, over the decades, Eulerian-Lagrangian approaches have successfully been applied to the simulation of the behaviour of microbubbles in turbulence (Wang & Maxey 1993; Spelt & Biesheuvel 1997; Mazzitelli et al. 2002, 2003; Snyder et al. 2007)

In this work, an Eulerian-Lagrangian model, where direct numerical simulation (DNS) is used to predict the liquid phase flow field, is developed and applied to bubbly flows in a vertical channel. In DNS all the continuum flow length and time scales are resolved, and it is used here to gain understanding of the complex physical phenomena occurring down to the smallest length scales. The knowledge generated through such studies is being increasingly used to improve the closure relations that are employed in more macroscopic treatments, such as the Eulerian-Eulerian multi-fluid model (Deen et al. 2004). In the context of bubbly flows, DNS has started to be applied only

relatively recently since the growth of HPC has made it affordable (Rasquin et al. 2014).

The DNS solver is coupled to a Lagrangian particle tracking routine that computes the trajectory of each bubble in the flow. The aim of the work is to evaluate the accuracy of the overall method for the effective prediction of bubble dynamics and interactions in turbulent flows, and the impact of the fluid flow turbulence on bubble coalescence and bubble size evolution. The model is initially validated against literature results for one-way and two-way coupled flows with microbubbles having diameters of 110 μm and 220 μm. This size range is of relevance to multiple engineering applications, such as the treatment of waste water and sewage with microbubbles of 150 μm that separate particulates from potable water, taking advantage of the high surface area to volume ratio of these bubbles (Wen et al. 2011). Subsequently, the model is extended to four-way coupling with the addition of a specific model to evaluate bubble collision and coalescence. The capabilities of the four-way coupled model are evaluated in a channel upflow and downflow of water at $Re_\tau$ = 150 with microbubbles having diameters of 110 μm.

**Numerical Approach**

To resolve turbulence dynamics down to the smallest scales, DNS relies on accurate algorithms that have maximum efficiency and low numerical dissipation, and fine space and time discretization. In this work, the high order spectral element Nek5000 code (Fischer et al. 2008) is used. The code solves the governing continuity and momentum balance equations for the fluid phase, which are written in non-dimensional form as below.

Non-dimensional continuity equation:

$$\nabla \cdot u^* = 0 \tag{1}$$

Non-dimensional momentum equation:

$$\frac{\partial u^*}{\partial t^*} + (u^* \cdot \nabla)u^* = -\nabla p^* + \frac{1}{Re_B}\nabla^2 u^* + f_i^* \tag{2}$$

Here, $f_i^*$ is an arbitrary forcing term that incorporates the imposed pressure gradient used to drive the single-phase flow and feedback from the bubbles to the fluid phase. $u^*$ and $p^*$ are the non-dimensional velocity and pressure, respectively. All the parameters are normalized by using the half-channel width $\delta$ as the reference length scale, and the bulk velocity $U_b$ as the reference velocity scale, which results in the reference time scale being $\delta/U_b$.

The flow domain studied is a vertical channel, modelled with two parallel walls. The size of the computational domain is $4\pi\delta \times 2\pi\delta \times 2\delta$, and it is discretized into 27×18×23 elements and 5.7 million Gauss-Lobatto-Legendre (GLL) grid-points using 8$^{th}$ order spectral elements. The grid resolution is comparable to, or higher than, other available literature studies of the same flow condition (Giusti et al. 2005; Molin et al. 2012). Streamwise, wall-normal and spanwise directions are denoted by *x*, *y* and *z*, and periodic conditions were assumed in both the streamwise and spanwise directions. The no-slip condition was imposed at the walls and the flow was driven by an imposed pressure gradient in the streamwise direction determined from the Reynolds number.

In order to model the transport of the dispersed phase, a Lagrangian bubble tracking routine was developed and interfaced with Nek5000. The tracker solves the non-dimensional form of Newton's second law equation of motion for each bubble, using a timestep equal to that of the fluid flow solver. Forces acting on the bubble are drag, lift, virtual mass, pressure gradient, gravity and buoyancy:

$$\begin{aligned}\rho_b^* \frac{du_{bi}^*}{dt^*} = {} & \frac{C_D}{\tau_b}\frac{1}{\rho_b^*}\left|u_{fi}^* - u_{bi}^*\right|\left(u_{fi}^* - u_{bi}^*\right) + (1-\rho_b^*)\frac{1}{Fr} \\ & + C_{VM}\left(\frac{Du_{fi}^*}{Dt^*} - \frac{du_{bi}^*}{dt^*}\right) + \frac{Du_{fi}^*}{Dt^*} + C_L\left(u_{fi}^* - u_{bi}^*\right)\frac{\partial u_{fi}^*}{\partial x^*}\end{aligned} \tag{3}$$

where $\rho_b^*$ is the non-dimensional bubble density, $u_{fi}^*$ and $u_{bi}^*$ are the non-dimensional fluid and bubble velocity, $C_D$ is the drag coefficient, $\tau_b$ the bubble response time, *Fr* the Froude number, $C_{VM}$ the virtual mass coefficient and $C_L$ the lift coefficient. Two-way coupling was achieved by including feedback from each bubble to the fluid phase through $f_i^*$ in the momentum conservation equation (Eq. (2)).

In four-way coupled simulations, bubble-bubble interactions are also accounted for because, when the bubble concentration is sufficiently high, the number of bubble collisions increases significantly and can no longer be neglected. In this work, only binary collisions were considered and these were modelled with a hard sphere collision approach. When two bubbles collide, therefore, there are two possible outcomes, i.e. the two bubbles merge and coalesce or they bounce off each other after the collision. Numerous models are available to determine whether the bubbles coalesce after they collide. These have been recently summarized in the comprehensive work of Liao and Lucas (2010). In this work, the film drainage model proposed by Prince and Blanch (1990) and the contact model of Sommerfeld et al. (2003) were adopted first. In addition, a different contact time model (Kamp et al. 2001) and the energy model (Sovová 1981) were also evaluated.

According to the film drainage model, when two bubbles collide a thin liquid film remains trapped between them (Chesters 1991; Oolman and Blanch 1986). Coalescence only happens if the interaction between the bubbles lasts long enough to allow the liquid to drain and the film to thin down to a thickness at which bubble rupture occurs. In the model, this happens only when the bubble contact time $t_{contact}$ is greater than the film drainage time $t_{drainage}$. The contact time was modelled according to Sommerfeld et al. (2003):

(4)

$$t_{contact} = \frac{C_c r_{eq}}{u_n}$$

Here, $r_{eq}$ is an equivalent bubble radius of two colliding unequal sized bubbles of $r_1$ and $r_2$. $C_c$ is a constant that determines the deformation distance as a fraction of the effective bubble radius and $u_n$ is the normal component of the relative impact velocity.The drainage time was taken from Prince and Blanch (1994):

$$t_{drainage} = \sqrt{\frac{{r_{eq}}^3 \rho_C}{16\sigma}}\, ln\left(\frac{h_0}{h_f}\right) \quad (5)$$

where $\sigma$ is the surface tension and $\rho_c$ the density of the continuous fluid phase. For an air-water system, the initial film thickness $h_0$ and the final thickness before rupture $h_f$ were taken to be $10^{-4}$ m and $10^{-8}$ m, respectively. The contact time from Kamp et al. (2001) was also tested. In their model, the contact time is expressed from a balance between the increasing surface free energy and the corresponding reduction in the kinetic energy of the system:

$$t_{contact} = \frac{\pi}{4}\left(\frac{8\rho_c C_{VM} r_{eq}^3}{3\sigma}\right)^{1/2} \quad (6)$$

The energy model was firstly developed by Howarth (1964, 1967). In this model, coalescence depends on the impact of the colliding bubbles, i.e. the relative velocity of two colliding bubbles should be larger than a critical value. Based on this, Sovová (1981) proposed the energetic collision model, in which coalescence occurs if the kinetic collision energy $E_{kin}$ exceeds the surface energy $E_s$:

$$E_s = 4\sigma\left(\frac{\pi}{6}\right)^{2/3}(r_1^2 + r_2^2) \quad (7)$$

$$E_{kin} = \frac{2\pi}{3}\rho_g u_{rel}^2 \frac{r_1^3 r_2^3}{r_1^3 + r_2^3} \quad (8)$$

The new bubble's radius after coalescence was calculated from a volume balance:

$$r_{new} = ({r_1}^3 + {r_2}^3)^{1/2} \quad (9)$$

Initially, a single-phase flow at $Re_\tau$ = 150 was simulated until a statistically steady-state was reached. Then, a total of 181,340 and 22,659 bubbles of diameters $d_b$ = 110 μm and 220 μm, respectively, were injected for the one-way and two-way coupled cases. The number of bubbles used corresponds to a void fraction of 0.01%, which is low enough for bubble-bubble interactions to be neglected. The bubbles were injected with a random spatial distribution in the fully developed turbulent channel flow, with the initial bubble velocities matching those of the fluid at the bubble centre. When a bubble reached a periodic boundary, it was re-injected at the corresponding boundary, keeping the average void fraction of the bubbles constant. Both upflow and downflow flow conditions were studied and the results validated against the DNS simulations of Giusti et al. (2005) and Molin et al. (2012).

After the validation, the number of 110 μm bubbles was increased to 1,928,513 for the four-way coupled case. This number was used to obtain a void fraction of 0.1%, necessary to record a significant number of bubble collisions.

**Results and Discussion**

The single-phase flow at shear Reynolds number $Re_\tau$ = 150 was validated against the DNS database of Molin et al. (2012). The computation was run until fully-developed conditions were reached. Once attained, the flow field was averaged until the mean flow statistics were independent of time. The instantaneous streamwise velocity in the channel is shown in Fig. 1, together with the GLL grid-points.

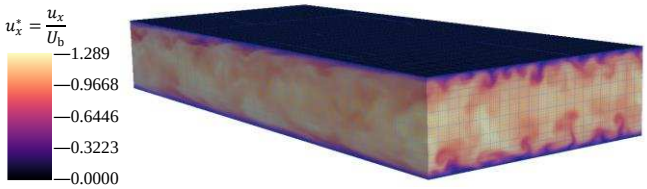


**Figure 1:** Computational mesh and non-dimensional instantaneous streamwise velocity in the channel for the single-phase flow at $Re_\tau$ = 150.

Time- and space-averaged Nek5000 results, normalized by the shear velocity (specified with the superscript $^+$, while $^*$ is used for variables normalized with bulk quantities), are compared with the predictions of Molin et al. (2012) in Fig. 2. Excellent agreement is obtained for the mean streamwise velocity in Fig. 2(a) and the root mean square (rms) of the velocity fluctuations and Reynolds shear stress in Fig. 2(b).

One-way and two-way coupled simulations with microbubbles of diameters $d_b$ = 110 μm and 220 μm were also successfully validated. Here, we present only the bubble distribution in the upflow channel with $d_b$ = 220 μm bubbles (Fig. 3). Driven by the lift force, small spherical bubbles accumulate near the wall of the channel, as shown in Fig. 3(b). Conversely, in downflow, since the bubbles travel more slowly than the fluid, the same lift force pushes the bubbles towards the centre of the channel. Fig. 3(a) shows the bubble distribution in the viscous sub-layer in upflow, superimposed on the velocity field. Clearly, the bubbles preferentially concentrate in regions of low fluid velocity.

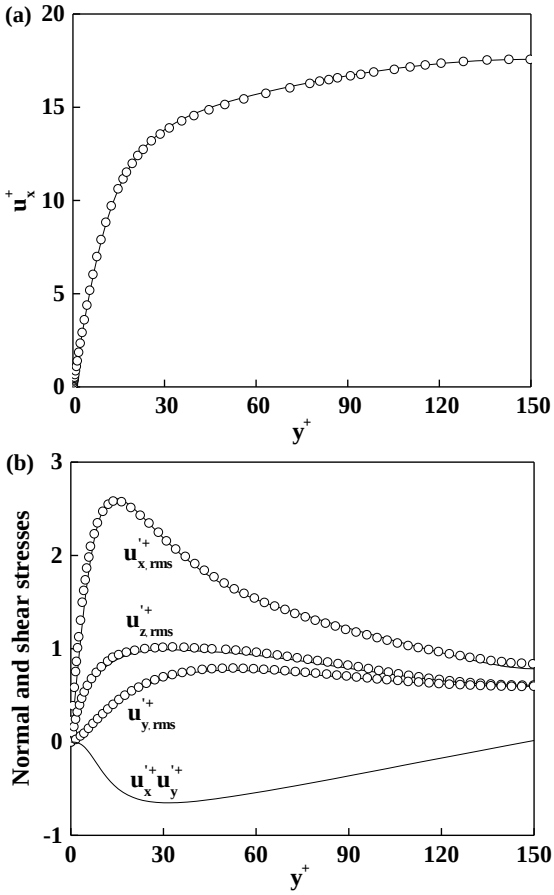


**Figure 2:** Comparison of single-phase fluid flow at $Re_\tau$ = 150 (—) with predictions of Molin et al., 2012 (○). (a) Mean streamwise fluid velocity ($u_x^+$); and (b) wall-normal ($u_{y,rms}^{\prime+}$), spanwise ($u_{z,rms}^{\prime+}$) and streamwise ($u_{x,rms}^{\prime+}$) rms of velocity fluctuations, and shear stress ($u_x^{\prime+}u_y^{\prime+}$).

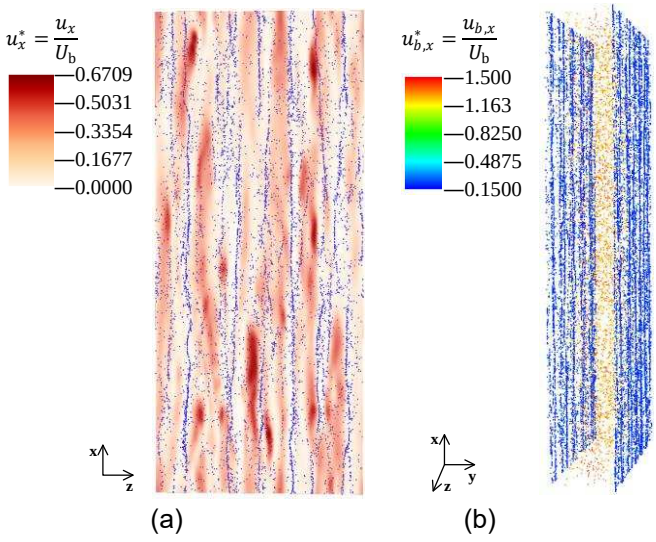


**Figure 3:** Instantaneous bubble distribution in upflow at $Re_\tau$ = 150 for $d_b$ = 220 μm bubbles. (a) Instantaneous bubble distribution in a thin slice of the viscous sub-layer with contour levels of fluid streamwise velocity; and (b) instantaneous bubble distribution with contour levels of bubble streamwise velocity in whole channel.

After successful validation, the four-way coupled model was applied to the upflow and the downflow conditions at $Re_\tau$ = 150 with $d_b$ = 110 μm bubbles, and a void fraction of 0.1%. The bubble mean velocity profiles, and normal and shear stresses, for both upflow and downflow are compared in Fig. 4. The bubble number density, normalized by its initial value, is also plotted as a function of the distance from the wall in Fig. 5. Under the effect of the lift force, more bubbles travel to the wall area in upflow with the bubble concentration peaking at the wall. Conversely, in downflow, more bubbles move towards the centre of the channel and a bubble depleted region is found close to the wall.

Figure 4(a) shows that, as expected, bubbles travel faster in upflow than in downflow. Similar levels of bubble normal and shear stresses are found in the two flows (Fig. 4(b)), except for the peaks in the near-wall region. There, the streamwise rms and the turbulent shear stress are higher in upflow. This follows from the tendency of the bubbles to enhance the fluid turbulence in upflow and suppress it in downflow. In the immediate vicinity of the wall, however, rms values in downflow tend to become higher, but this is a consequence of the small number of bubbles in this region that prevented statistically meaningful averaging. Therefore, additional results closer to the wall are not shown for the downflow case.

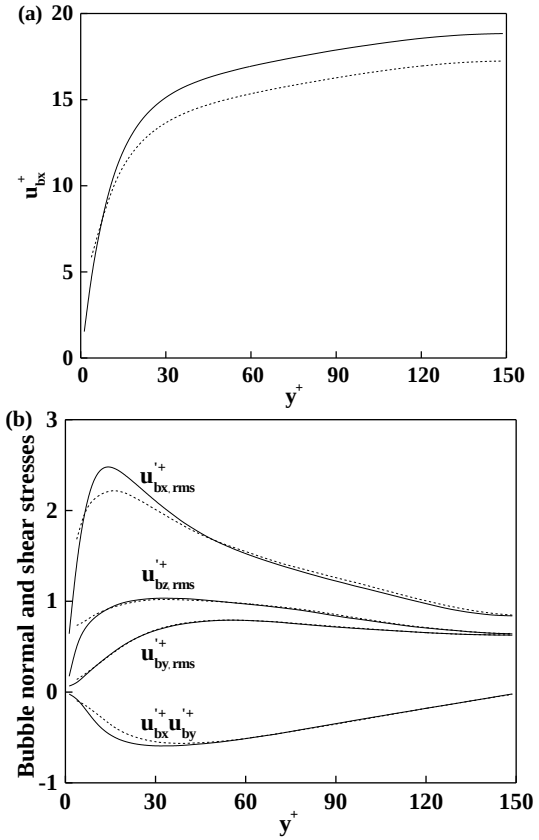


**Figure 4:** Bubble velocity statistics in four-way coupled upflow (—) and downflow (- - -) at $Re_\tau$ = 150 with $d_b$ = 110 bubbles. (a) Mean streamwise velocity ($u_{bx}^+$); and (b) wall-normal ($u_{by,rms}^{\prime+}$), spanwise ($u_{bz,rms}^{\prime+}$) and streamwise ($u_{bx,rms}^{\prime+}$) rms of velocity fluctuations, and shear stress ($u_{bx}^{\prime+}u_{by}^{\prime+}$).

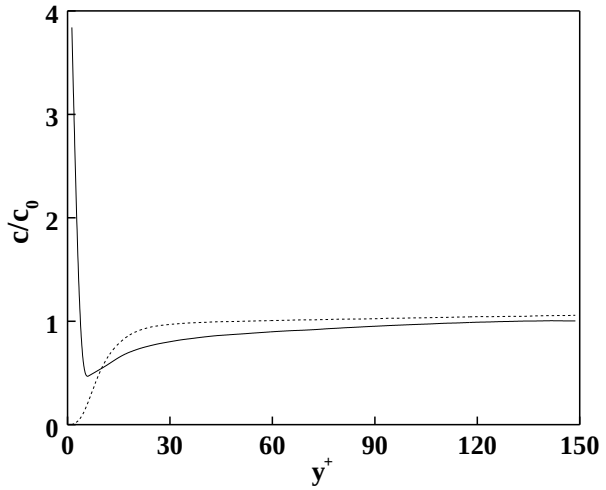


**Figure 5:** Four-way coupled bubble number density profiles normalized by the initial bubble concentration in upflow (—) and downflow (- - -) at $Re_\tau$ = 150 with $d_b$ = 110 μm bubbles.

Collision and coalescence events were recorded and their distribution in the wall-normal direction is presented in Fig. 6. Because of the high concentration of bubbles near the channel walls in upflow, more collisions are found in these regions than in the channel centre, as shown in Fig. 6(a). Since this occurs not only in upflow, but also in downflow, the peaks are also due to higher levels of turbulence in these regions promoting collisions. In contrast with the upflow, the number of collisions in downflow decreases again in the very near-wall region (Fig. 6(b)), because of the small number of bubbles in these regions.

In Fig. 6, the coalescence efficiencies are found to be 100% in both cases, such that every collision in the channel results in a coalescence. These results were obtained using the model of Sommerfeld et al. (2003), which estimates the bubble contact time from the time taken by a bubble with a certain relative collision velocity to travel a distance equal to a specified fraction of the bubble radius. This fraction is arbitrarily set to 0.25, and deceleration of the bubble during the collision process is neglected. Hence, the model of Kamp et al. (2001) was also tested. The results, however, also showed the same 100% efficiency in both flows, since the contact time between the bubbles was always long enough to allow drainage of the liquid film trapped between them. In contrast, the results changed completely when using the energy model, where 0% coalescence efficiency was found, suggesting further investigation into the accuracy of different coalescence models is desirable.

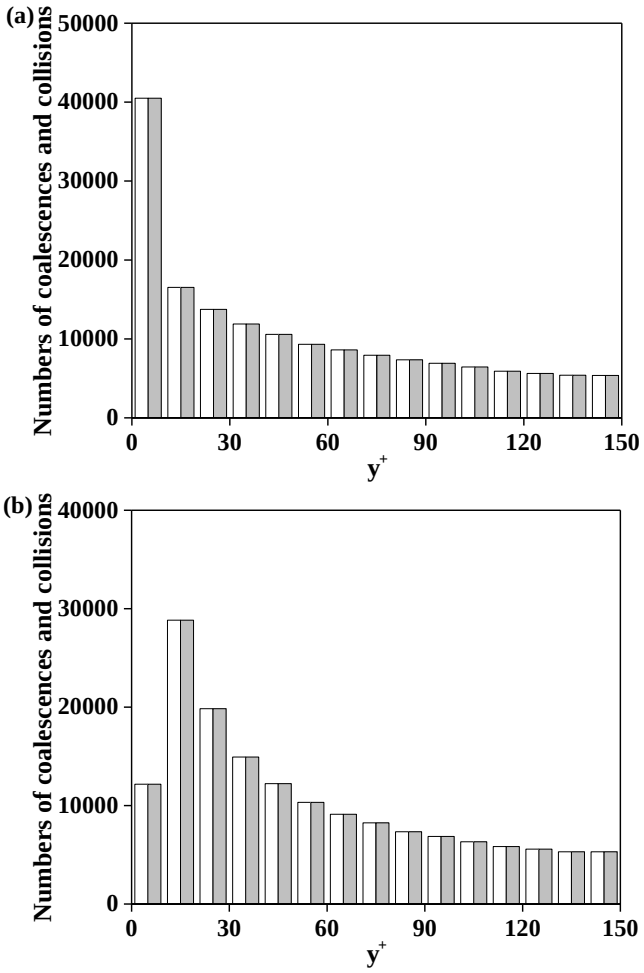


**Figure 6:** Number of bubble collisions (□) and coalescences (■) in the wall-normal direction in (a) upflow and (b) downflow at $Re_\tau$ = 150 with $d_b$ = 110 μm bubbles.

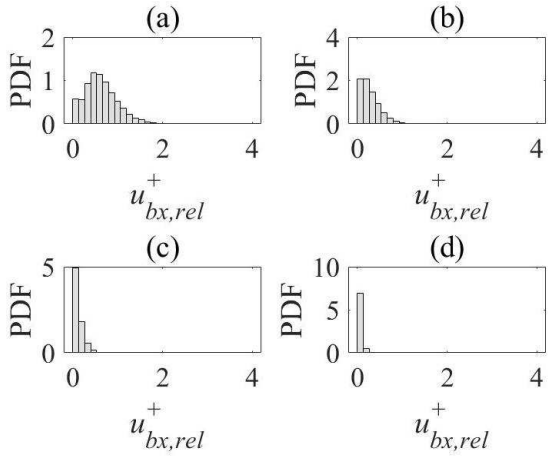


**Figure 7:** PDF of relative bubble collision velocities in different regions of the channel in upflow at $Re_\tau$ = 150 with $d_b$ = 110 μm bubbles. (a) Viscous sub-layer; (b) buffer region; (c) log-law region; and (d) bulk flow region.

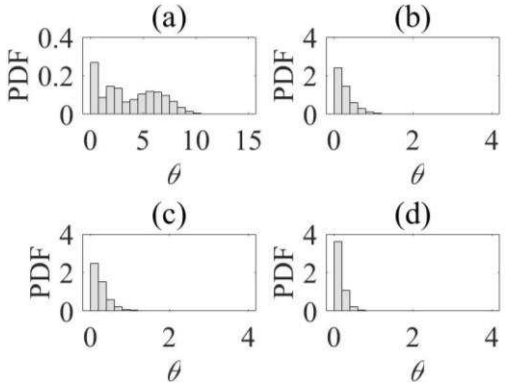


**Figure 8:** PDF of bubble collision angles in different regions of the channel in upflow at $Re_\tau$ = 150 with $d_b$ = 110 μm bubbles. (a) Viscous sub-layer; (b) buffer region; (c) log-law region; (d) bulk flow region.

An explanation for the 100% efficiency of the film drainage model (and 0% for the energy model) is found in the results of Figs. 7 and 8. In Fig. 7, the relative bubble collision velocities in the streamwise direction are plotted in different regions of channel. In Fig. 8, the same is done for the bubble collision angles. The relative velocities, and angles, are always very small, with the highest values found in the viscous sub-layer where the largest mean velocity gradients, but the lowest turbulence levels, are found. At the shear Reynolds number considered, turbulence affects bubble motion mainly in the streamwise direction, resulting in collisions that are almost rectilinear and with streamwise-only relative velocities (collision velocities in the other two directions are not plotted due to their small values). As a consequence of the type of collision, the predicted contact time is always high, which explains the 100% efficiency returned by the film drainage model. Conversely, the low relative velocity translates into low-energy collisions, explaining the 0 % efficiency of the energy model.

## Conclusions

Turbulent upward and downward flows of microbubbles in a channel were studied using a four-way coupled Eulerian-Lagrangian approach. The accuracy of the model was successfully validated against single-phase and two-way coupled literature results. The four-way coupled model provides a quantitative description of microbubble dynamics, and clarifies the mechanisms of bubble collision and coalescence driven by the continuous fluid flow field. At the levels of turbulence investigated, collisions mainly occur on quasi-rectilinear bubble trajectories. Therefore, the angle of collision is usually very small and the relative approach velocity between the two colliding bubbles is generally low. These low-energy collisions favour the film drainage coalescence model over the energy model, but the contradictory predictions from these two approaches warrants further investigation. The understanding generated on the dynamics of bubble-bubble interactions is of value to the development of coalescence models, and the closure relations used in macroscopic Eulerian-Eulerian approaches.

## Acknowledgments

JZ gratefully acknowledges funding through an Anniversary Research Scholarship from the University of Leeds.

## References

Balachandar, S. & Eaton, J.K. Turbulent dispersed multiphase flow. Annu. Rev. Fluid Mech., Vol. 42, pp.111-133 (2010)

Chesters, A.K. Modelling of coalescence processes in fluid-liquid dispersions: A review of current understanding. Chem. Eng. Res. Des., Vol. 69, pp. 259-270 (1991)

Deen, N.G., van Sint Annaland M. & Kuipers J.A.M. Multi-scale modeling of dispersed gas-liquid two-phase flow. Chem. Eng. Sci., Vol. 59, pp. 1853-1861 (2004)

Elghobashi, S. On predicting particle-laden turbulent flows. Appl. Sci. Res., Vol. 52, pp. 309-329 (1994)

Fischer, P., Kerkemeier, J. & Stefan, G. Web page: http://nek5000.mcs.anl.gov. (2008)

Giusti, A., Lucci, F. & Soldati, A. Influence of the lift force in direct numerical simulation of upward/downward turbulent channel flow laden with surfactant contaminated microbubbles. Chem. Eng. Sci., Vol. 60, pp. 6176-6187 (2005)

Howarth, W.J. Coalescence of drops in a turbulent flow field. Chem. Eng. Sci., Vol. 19, pp. 33-38 (1964)

Howarth, W.J. Measurement of coalescence frequency in an agitated tank. AIChE J., Vol. 13, pp. 1007-1013 (1967)

Kamp, A.M., Chesters, A.K., Colin, C. & Fabre, J. Bubble coalescence in turbulent flows: A mechanistic model for turbulence-induced coalescence applied to microgravity bubbly pipe flow. Int. J. Multiphas. Flow, Vol. 27, pp. 1363-1396 (2001)

Lau, Y.M., Deen N.G. & Kuipers J.A.M. Development of an image measurement technique for size distribution in dense bubbly flows. Chem. Eng. Sci., Vol. 94, pp. 20-29 (2013)

Liao, Y. & Lucas, D. A literature review on mechanisms and models for the coalescence process of fluid particles. Chem. Eng. Sci., Vol. 65, pp. 2851-2864 (2010)

Mazzitelli, I.M., Lohse, D. & Toschi, F. The effect of microbubbles on developed turbulence. Phys. Fluids, Vol. 15, pp. L5-L8 (2002)

Mazzitelli, I.M., Lohse, D. & Toschi, F. On the relevance of the lift force in bubbly turbulence. J. Fluid Mech., Vol. 488, pp. 283-313 (2003)

Molin, D., Marchioli, C. & Soldati, A. Turbulence modulation and microbubble dynamics in vertical channel flow. Int. J. Multiphas. Flow, Vol. 42, pp. 80-95

(2012)

Oolman, T.O. & Blanch, H.W. Bubble coalescence in stagnant liquids. Chem. Eng. Commun., Vol. 43, pp. 237-261 (1986)

Prince, M.J. & Blanch, H.W. Bubble coalescence and break-up in air-sparged bubble columns. AIChE J., Vol. 36, pp. 1485-1499 (1990)

Rasquin, M., Smith, C., Chitale, K., Seeyoung Seol, E., Matthews, B.A., Martin, J.L., Sahni, O., Loy, R.M., Stephard, M.S. & Jansen, K.E. Scalable implicit flow solver for realistic wing simulations with flow control. Comput. Sci. Eng., Vol. 16, pp. 13-21 (2014)

Shah, Y.T., Kelkar, B.G., Godbole, S.P. & Deckwer, W.-D. Design parameters estimations for bubble column reactors. AIChE J., Vol. 28, pp. 353-379 (1982)

Snyder, M.R., Knio, O.M. & Katz J. Statistical analysis of small bubble dynamics in isotropic turbulence. Phys. Fluids, Vol. 19, 065108 (2007)

Sommerfeld, M., Bourloutski, E. & Bröder, D. Euler/Lagrange calculations of bubbly flows with consideration of bubble coalescence. Can. J. Chem. Eng., Vol. 81, pp. 508-518 (2003)

Sovová, H. Breakage and coalescence of drops in a batch stirred vessel − II Comparison of model and experiments. Chem. Eng. Sci., Vol. 36, pp. 1567-1573 (1981)

Spelt, P.D.M. & Biesheuvel, A. On the motion of gas bubbles in homogeneous isotropic turbulence. J. Fluid Mech., Vol. 336, pp. 221-244 (1997)

Todreas, N.E. & Kazimi M.S., Nuclear systems volume I: Thermal hydraulic fundamentals. 2011: CRC press (2011)

Wang, L.-P. & Maxey, M.R. The motion of microbubbles in a forced isotropic and homogeneous turbulence. Appl. Sci. Res., Vol. 51, pp. 291-296 (1993)

Wen, L.H., Ismail, A.B., Menon, P., Saththasivam, J., Thu, K. & Choon, N.K. Case studies of microbubbles in wastewater treatment. Desalin. Water Treat., Vol. 30, pp. 10-16 (2011)